REPORT NO. 413

COO-1469-0175

DESIGN FACTORS FOR A TRANSITION TEMPERATURE POCKELS TUBE

by

CHINLON LIN

August, 1970

DEPARTMENT OF COMPUTER SCIENCE
UNIVERSITY OF ILLINOIS AT URBANA-CHAMPAIGN · URBANA, ILLINOIS

REPORT NO. 413

DESIGN FACTORS FOR A TRANSITION TEMPERATURE POCKELS TUBE*

by

CHINLON LIN

August, 1970

Department of Computer Science
University of Illinois
Urbana, Illinois 61801

* Supported in part by Contract Number U.S. AEC AT(11-1) 1469 and submitted in partial fulfillment of the requirements for the degree of Master of Science in Computer Science at the University of Illinois, August, 1970.

ACKNOWLEDGMENT

The author is deeply indebted to his advisor, Professor Michael Faiman, for suggesting the subject and for constant guidance and counsel. He would also like to express thanks to Mr. Douglas Sand for discussions.

The author would also like to thank Miss Carla Donaldson for typing the manuscript.

This research was supported in part by the Atomic Energy Commission under Contract No. US AEC AT(11-1) 1469, W. J. Poppelbaum, Principal Investigator.

TABLE OF CONTENTS

LIST OF FIGURES

LIST OF TABLES

1. INTRODUCTION

Electro-optic modulation and deflection of light are based on the manipulations of the optical properties of crystals by means of external electric fields. The dependence of the phase velocity of light propagating in crystals on the applied electric field can be used to modulate the amplitude and phase of the light, and to control the direction of the light beam.[1]

In the electro-optic light valve, or Pockels tube, a charge distribution representing a video image is written on an electro-optic crystal, which modulates the light shining through by means of the longitudinal linear electro-optic (Pockels) effect. The field in the crystal caused by the charge pattern imposes a modulation across the wavefront of the incoming light beam, allowing not only an optical image to be obtained but also, if the light is coherent, its Fourier Transform. This has led to investigations in the use of the electro-optic light valve in a large screen television projection system[2] and in an on-line video information processing system.[3]

Various versions of the electro-optic light valve have been under development for years,[4,5,6,7] but none of them was capable of giving resolution comparable to that of standard television. The resolution is primarily determined by the thickness of the crystal relative to the size of its faces[7]: the larger and thinner the crystal, the higher the resolution. For example, a 1" square crystal has to be polished to about 2 mils thick to give standard television resolution. However, the techniques of polishing make it difficult to produce large and thin enough crystals. In the On-line Video Processing System[3] developed by the Hardware Research Group, University of Illinois, Department of Computer Science, using a 1"

square, 5 mil KD*P crystal and operating at ambient temperature, the resolution obtainable has been about 200 lines.

Fortunately, it is possible to improve the resolution by utilizing the ferroelectric properties of materials such as KDP and KD*P. If the crystal temperature is maintained near its transition (Curie) temperature, the effective thickness of the crystal is reduced and the resolution is correspondingly increased. The advantages and various design considerations of this transition-temperature operation are the subjects of interest in this thesis.

2. ADVANTAGES OF TRANSITION TEMPERATURE OPERATION

KDP (KH_2PO_4) and KD*P (KD_2PO_4) are $\bar{4}2m$ class crystals which exhibit the linear electro-optic effect (Pockels effect).[1] They are also ferroelectric crystals for which a transition temperature T_c, also known as the Curie temperature, exists, such that above it the crystal is paraelectric while below it the crystal is ferroelectric. Within the vicinity of T_c the dielectric constant of the crystal along the c-axis, ϵ_c, can attain very high values. Above the transition temperature, ϵ_c follows the Curie-Weiss law:

$$\epsilon_c = \frac{A}{T - T_0} + B$$

where A and B are constants and T_0 is called the Curie-Weiss temperature.[8,9] In this equation B is about two orders of magnitude smaller than A, so that a plot of $1/\epsilon_c$ versus temperature is a virtually straight line. T_0 is the extrapolation of this line to the temperature axis. In general, T_0 differs from T_c, especially for ferroelectrics which undergo a first order transition.[10,11] For materials exhibiting a second order transition, T_0 is almost the same as T_c. But the important feature here is that as the Curie temperature is approached, ϵ_c attains extremely large values. Using this property, there are several advantages in operating with the crystal cooled down to its transition temperature, rather than at ambient temperature, as described in Reference 3.

1) The half-wave voltage, the voltage required to produce a phase retardation of π, is greatly lowered. In the longitudinal linear electro-optic effect the induced phase retardation of the light passing through the

crystal is given by[1]

$$\Gamma = \pi \frac{V}{V_\pi}$$

where the half-wave voltage V_π is

$$V_\pi = \frac{\lambda_0}{2n_a^3 r_{63}} \tag{1}$$

V is the applied voltage; λ_0 is the wavelength of the incident light; n_a is the index of refraction for the "ordinary ray", and r_{63} is an element of the electro-optic tensor. r_{63} is essentially proportional to $\epsilon_c - 1$, where ϵ_c is the dielectric constant along the c-axis.[13]

Near the transition temperature ϵ_c is much larger than at room temperature. Therefore, V_π, which is inversely proportional to r_{63}, decreases considerably as r_{63} rises. Hence it allows the use of a much lower control voltage and the associated electronics will be much simpler since an electron beam of lower velocity can be used.

2) The effective crystal thickness is considerably reduced. As mentioned above, the resolution is primarily determined by the crystal thickness. A detailed analysis[14] has shown that the effective crystal thickness T' is determined by the ratio of the dielectric constants, by the following relation:

$$T' = T\left(\frac{\epsilon_a}{\epsilon_c}\right)^{\frac{1}{2}} \tag{2}$$

where T is the true thickness of the crystal. At ambient temperature ϵ_c and ϵ_a have the same order of magnitude. This requires that the thickness of

the crystal plate be less than the size of the charge spot, since otherwise the lines of force of the applied electric field would greatly deviate from the direction of the c-axis if the crystal is thick. At the transition temperature of the crystal, the situation is different. ϵ_c can be as much as 10 times greater than ϵ_a near the transition temperature. Consequently, the same resolution can be achieved using a thicker crystal, or equivalently, better resolution is attainable with a crystal of the same thickness.

3) The time constants of the crystal are greatly increased. The charge spread between points of different voltage over the crystal surface is due to the finite resistivity of the crystal. The time constant at which the charge spreads in the direction of the a-axis is

$$\tau' = \epsilon_0 \epsilon_a \rho_a \tag{3}$$

where ρ_a is the crystal resistivity in the direction of the a-axis. Similarly, the time constant in the c-direction, through the crystal thickness, is

$$\tau = \epsilon_0 \epsilon_c \rho_c \tag{4}$$

where ρ_c is crystal resistivity in the direction of the c-axis. The charge spread across the crystal surface affects the resolution by the so-called diffusion effect; the charge leakage through the crystal thickness causes a loss of contrast.

Both ρ_a and ρ_c increase as the temperature decreases. Hence, as the temperature is lowered down to the transition temperature, ρ_a, ρ_c, and ϵ_c increase considerably, giving much larger time constants. This gives a

more stable charge pattern since there is less charge spread in a given time interval. On the one hand a flicker-free image, or even information storage, is possible because of this high time constant; on the other hand the problem has become that of erasure, the removal of the previous charge pattern, instead of that of stablizing the written charge pattern.

These significant advantages have motivated the investigation of the problems associated with the transition temperature operation of an electro-optic light valve to be used in video information processing systems. Various design considerations concerning this transition-temperature operation are discussed in the following chapters.

3. ELECTRO-OPTIC PROPERTIES OF KDP AND KD*P

Crystals of KDP and its isomorphs have been widely used for light modulation, switching and deflection because of their relatively large electro-optic coefficients and their availability in large samples of satisfactory optical quality. The deuterated version, KD*P, has the largest electro-optic coefficients, but is more expensive to manufacture.

KDP and KD*P crystals are negative uniaxial, namely $n_a = n_b > n_c$. They possess a $\bar{4}2m$ point-group symmetry, so that the only non-vanishing components of their electro-optic tensor are $r_{41} = r_{52}$ and r_{63}.[1] In the presence of an electric field, therefore, the index ellipsoid takes the form:

$$\frac{1}{n_a^2}(x^2 + y^2) + \frac{1}{n_c^2} z^2 + 2r_{41}(E_x y + E_y x)z + 2r_{63}E_z xy = 1 \qquad (5)$$

When the field is along the z-axis, this simplifies to

$$\frac{1}{n_a^2}(x^2 + y^2) + \frac{1}{n_c^2} z^2 + 2r_{63}E_z xy = 1 \qquad (6)$$

Transforming to principal axes via

$$x = \frac{1}{\sqrt{2}}(x' - y'),\ y = \frac{1}{\sqrt{2}}(x' + y') \text{ and } z = z'$$

then yields

$$\frac{x'^2}{n_a'^2} + \frac{y'^2}{n_b'^2} + \frac{z'^2}{n_c'^2} = 1 \qquad (7)$$

where

$$n'_a = n_a - \frac{1}{2}n_a^3 r_{63} E_z,$$

$$n'_b = n_a + \frac{1}{2}n_a^3 r_{63} E_z, \tag{8}$$

$$n'_c = n_c$$

and use has been made of the fact that $r_{63}E_z \ll \frac{1}{n^2}$.

This is the well known result that the presence of the electric field E_z makes the formerly uniaxial crystal biaxial, with x' and y' being the fast and slow axes, respectively. Thus, for light of wavelength λ_0 propagating in the z direction through a crystal of thickness t, the relative phase change between x' and y' polarizations is

$$\Gamma = \frac{2\pi}{\lambda_0} n_a^3 r_{63} E_z t = \pi \frac{V}{V_\pi} \tag{9}$$

where $V = E_z t$ is the applied voltage, and V_π is the half-wave voltage given by

$$V_\pi = \frac{\lambda_0}{2n_a^3 r_{63}} \tag{10}$$

as noted previously in Chapter 2.

KDP and KD*P are also ferroelectric crystals. Their dielectric constant ϵ_c follows the Curie-Weiss law above the transition temperature[15]:

$$\epsilon_c = 4.5 + \frac{3122}{T - T_0} \tag{11}$$

Figure 1 shows ϵ_c and ϵ_a of KDP versus temperature.[16]

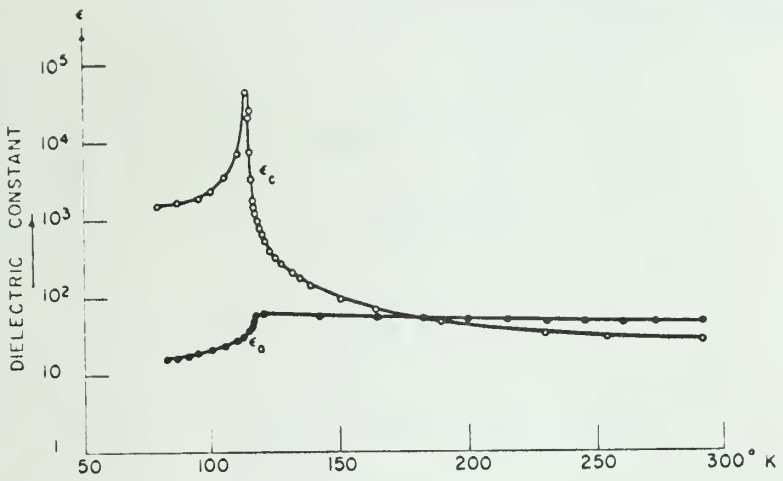

Figure 1. Dielectric Constants of KDP as a Function of Temperature

The effect of deuteration is essentially the shift of the transition temperature.[12,17] For partially deuterated KDP, i.e., $KD_{2x}H_{2(1-x)}PO_4$, the following expression approximately gives the effect of deuteration on the transition temperature[12]:

$$T_c = (123 + 106x)^\circ K \tag{12}$$

For pure KDP, x = 0, T_c is 123°K.[16] For 100% deuterated KDP, i.e., pure KD*P, T_c is 229°K from the above expression. The reported experimental values of T_c for KD*P have been 213°K and 222°K. The latter value is believed to be nearer to that of pure KD*P.[17] A KD*P sample with a transition temperature of 222°K has been analyzed, using nuclear magnetic resonance, to have 91% deuteration, though the starting solution for

preparing this sample was 99% deuterated.[12] This probably is the highest transition temperature for commercially available KD*P.

The resistivities of KDP are expressed by[15]

$$\log_{10} \rho_c = 1.27 + \frac{2740}{T} \text{ ohm - cm}$$
$$\log_{10} \rho_a = 1.85 + \frac{2470}{T} \text{ ohm - cm} \qquad (13)$$

where T is in ^{o}K. They are shown in Figure 2. These are for KDP and seem to be valid for the temperature range above T_c only. According to Mason[15], these curves assume H-bond related ionic conductivity, which would imply: 1) deuteration should change the resistivity values; 2) extension of the expressions down near the transition temperature is questionable. However, since precise values are not needed here, these expressions will still be used in calculations of the time constants, the result of which is intended only to indicate the large increase of time constants for the transition temperature operation.

The ratio $r_{63}/(\epsilon_c - 1)$ is essentially temperature independent.[13] In other words, r_{63} has Curie-Weiss temperature dependence. Figure 3 shows the electro-optic tensor element r_{63} as a function of temperature for both KDP and KD*P crystals.[13]

Using the figures and the relations given above one can calculate various parameters such as half-wave voltage, effective crystal thickness, and time constants. However, the curves for ϵ_c and r_{63} given above are for "unclamped" crystals, while it has been known that a "clamped" crystal behaves differently in some respects. For the clamped crystal the dielectric

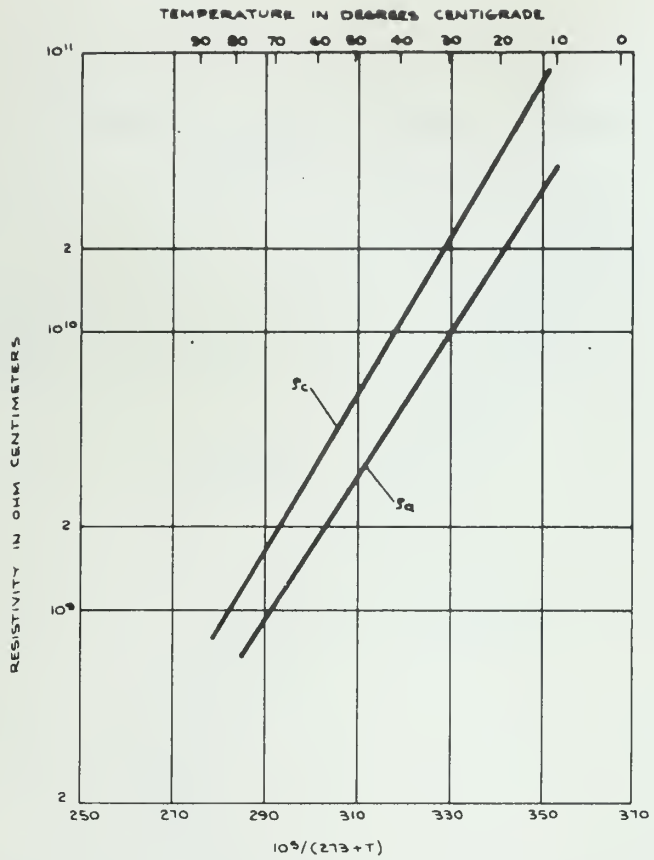

Figure 2. Resistivities of KDP as a Function of Temperature

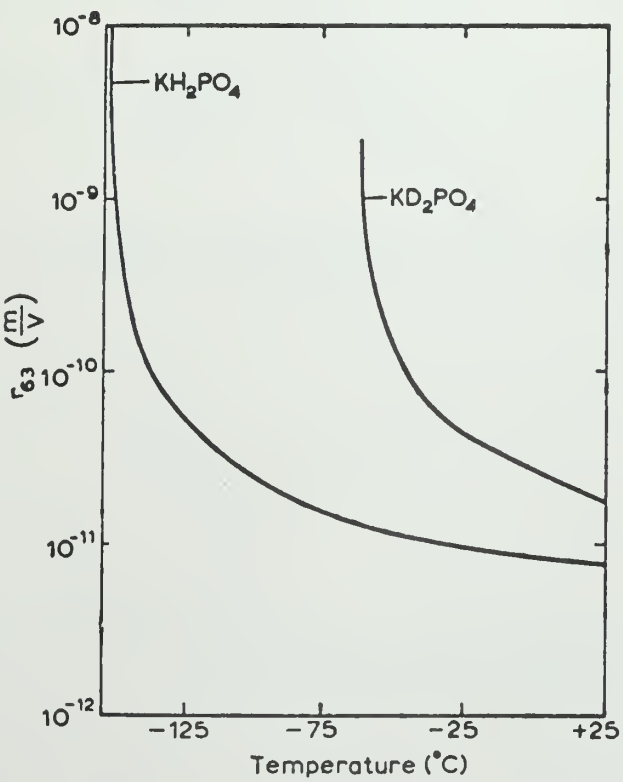

Figure 3. Electro-optic Tensor Element r_{63} of Unclamped KDP and KD*P as a Function of Temperature

constant ϵ_c above the transition temperature also follows the Curie-Weiss law but with a Curie-Weiss temperature about $4^{\circ}K$ lower than that of a free crystal for KDP,[18] and about $6.7^{\circ}K$ lower in the case of KD*P.[19] Figure 4 and Figure 5 show the reciprocal of the dielectric constants of KDP and KD*P as a function of temperature, for both clamped and unclamped cases.[18,19]

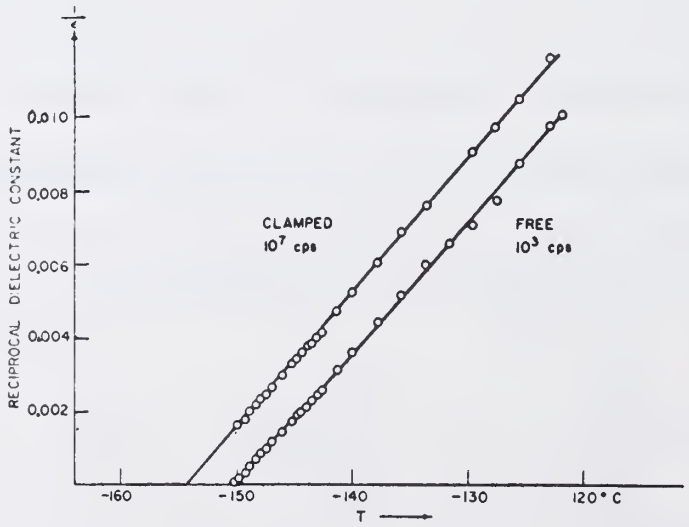

Figure 4. Reciprocal Dielectric Constant $1/\epsilon_c$ versus Temperature, Clamped and Unclamped KDP

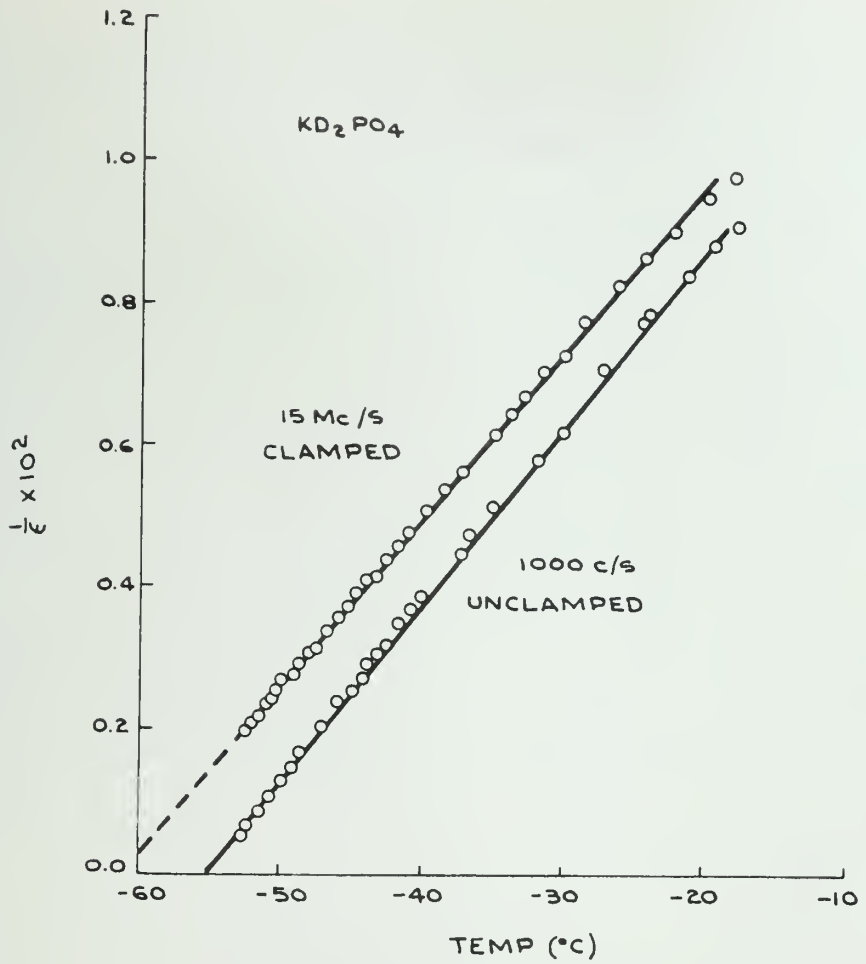

Figure 5. Reciprocal Dielectric Constant $1/\epsilon_c$ versus Temperature, Clamped and Unclamped KD*P

In these figures the "clamped" values are obtained by measurements at frequencies above the piezoelectric dispersion frequency, so that mechanical resonances are suppressed and the crystal is clamped by inertia.[8] For unclamped KDP, the Curie-Weiss temperature T_0 is practically the same as the transition temperature T_c, and is -150°C. For this particular unclamped KD*P the Curie-Weiss temperature T_0 is -54.8°C while the transition temperature T_c is -52.5°C. For clamped crystals the Curie-Weiss temperatures are shifted to -61.5°C for KD*P and -154°C for KDP, but the transition temperatures are the same as those of unclamped crystals. The reason is that, since clamping

by inertia cannot prevent the piezoelectric strain due to the spontaneous polarization (the so-called "spontaneous strain"), the transition takes place at the original transition temperature of the free crystal.[9]

It is not possible to verify the Curie-Weiss law for clamped crystals for temperatures between the transition point and the Curie-Weiss temperature with the high frequency method. Figure 6 shows the dielectric constant ϵ_c versus $T - T_c$, both in logarithmic scales, obtained from the results of measurements using unclamped and physically clamped KDP and KD*P crystals.[20] T_0 for the clamped case is, of course, different from T_0 for the unclamped case. This figure shows that, near the transition temperatures of KDP and KD*P, ϵ_c of free crystal plates can attain a maximum of about 4000 while that of fastened plates has only a maximum of about 650, the latter being the case of interest.

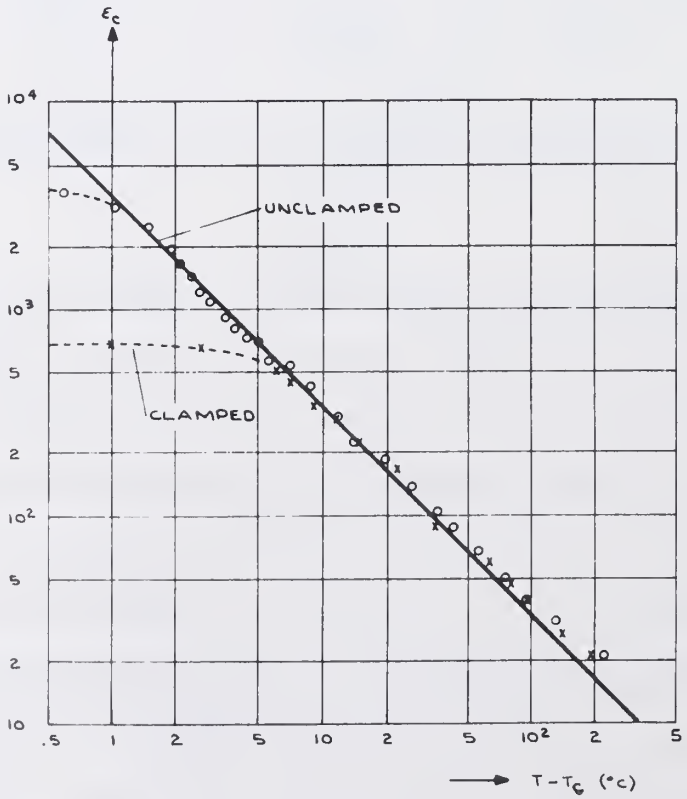

Figure 6. Dielectric Constants of KDP and KD*P Versus $T - T_c$, Unclamped and Clamped

The dielectric constant for the unclamped case is usually denoted by ϵ_c^T while that for the clamped case is ϵ_c^S, superscript T indicating constant stress and S constant strain.[21] The Curie-Weiss expression for ϵ_c^S, when applicable, is practically the same as that for ϵ_c^T except for a different Curie-Weiss temperature, T_0, as can be seen from Figures 4, 5 and 6.

For the clamped case, the computed data of various parameters for KDP and KD*P at different temperatures are given in Table 1. ϵ_c is read from Figure 6 in the nonlinear region while in the linear region equation (11) is approximately applicable and is hence used.

If the transition temperatures of KDP and KD*P are -150°C (123°K) and -51°C (222°K) respectively, and if we assume T_c is practically the same as T_0 for KDP type ferroelectrics, then reasonable values of T_0 for the calculation of ϵ_c^S are

$$\text{KDP:} \quad T_0 = -154^\circ\text{C} = 119^\circ\text{K}$$
$$\text{KD*P:} \quad T_0 = -55^\circ\text{C} = 218^\circ\text{K}$$

where T_0 is assumed to shift four degrees from the unclamped value, which, for KD*P, is not verified but reasonable enough, as T_0 will vary with the amount of deuteration.

The time constants τ' and τ are computed using equations (3) and (4), where ρ_a and ρ_c are obtained from (13), though, as mentioned, the extension to KD*P and down to the transition temperature might be questionable. ϵ_0 is the permittivity of free space, and is $8.854 \cdot 10^{-12}$ farad/meter. The effective crystal thickness is related to the true thickness by equation (2), where ϵ_a is obtained from the curves given in Reference 12.

KDP $T_0 = -154^{\circ}C$

$t^{\circ}C$	25	0	-50	-100	-140	-148	-152
ϵ_a	44	46	52	56	60	61	61
ϵ_c	21.9	24.8	34.5	62.3	227	523	650
ρ_a Ω - cm	1.35×10^{10}	7.76×10^{10}	8.32×10^{12}	1.15×10^{16}	2.63×10^{20}	4.07×10^{21}	1.82×10^{22}
ρ_c Ω - cm	2.88×10^{10}	2.0×10^{11}	3.63×10^{13}	1.26×10^{17}	7.41×10^{21}	1.55×10^{23}	8.13×10^{23}
τ sec	0.056	0.44	110	6.9×10^{5}	1.48×10^{11}	7.21×10^{12}	4.64×10^{13}
τ' sec	0.053	0.32	38.3	5.7×10^{4}	1.4×10^{9}	2.18×10^{10}	9.7×10^{10}
T'/T	1.41	1.36	1.23	0.95	0.515	0.34	0.307
r_{63} m/v	11.3×10^{-12}	12.9×10^{-12}	18.1×10^{-12}	33.2×10^{-12}	12.2×10^{-11}	28.2×10^{-11}	35.0×10^{-11}
V_π at λ_0	6210	5430	3870	2120	575	249	201
V_π at λ_0'	8170	7150	5100	2780	757	327	263

$\lambda_0 = 4880$ Å, $\lambda_0' = 6328$ Å

Table 1. Time Constants, Effective Thickness, and Half-Wave Voltages of KDP and KD*P at Different Temperatures, Clamped Case

Table 1 - continued

KD*P $T_0 = -55^{\circ}C$

$t^{\circ}C$	25	0	-25	-40	-50	-52
ϵ_a	60	62	64	64	65	65
ϵ_c	43.5	61.3	109	213	629	650
ρ_a Ω - cm	1.35×10^{10}	7.76×10^{10}	6.31×10^{11}	2.82×10^{12}	8.32×10^{12}	1.07×10^{13}
ρ_c Ω - cm	2.88×10^{10}	2.0×10^{11}	2.04×10^{12}	1.05×10^{13}	3.63×10^{13}	4.68×10^{13}
τ sec	0.111	1.10	19.6	198	2030	2700
τ' sec	0.072	0.43	3.55	15.4	48	61
T'/T	1.17	1.01	0.765	0.55	0.32	0.316
r_{63} m/v	23×10^{-12}	33×10^{-12}	58.3×10^{-12}	11.5×10^{-11}	34×10^{-11}	35×10^{-11}
V_π at λ_0	3070	2140	1220	620	208	202
V_π at λ_0'	4010	2850	1580	800	272	263

$\lambda_0 = 4880$ Å, $\lambda_0' = 6328$ Å

The half-wave voltage, V_π, is obtained using equation (1), where λ_0, r_{63}, and n_a are obtained as follows:

1) Wavelengths 4880Å (Argon ion laser) and 6328Å (Helium-Neon laser) are chosen for calculations.

2) As mentioned above, $r_{63}^T/(\epsilon_c^T - 1)\epsilon_0$ is temperature independent. The value of this ratio used here is 0.061 m^2/coulomb.[17] It has been pointed out that r_{63}^S is about 8% less than r_{63}^T for both KDP and KD*P, and the expression relating these two is available.[15,17] However, here we simply assume

$$r_{63}^S = 0.061(\epsilon_c^S - 1)\epsilon_0 \qquad (14)$$

3) The temperature dependence of the indices of refraction of KDP and KD*P, being very small, is not included. In cases when a high accuracy calculation is needed, more accurate data of the clamped r_{63} should be used and the temperature variation of the indices of refraction should be included. The temperature change of the indices of refraction from room temperature down near the transition temperatures of KDP and KD*P can be obtained from the following empirical formula[22]:

$$\Delta n = (n^2 + B)(298 - T)C \qquad T \text{ in } {}^\circ K \qquad (15)$$

where n is the reference value at 298°K and B, C are shown below:

		B	$C.10^4$
KDP	n_a	-1.432	0.402
	n_c	-1.105	0.221
KD*P	n_a	-1.047	0.228
	n_c	0	0.0955

The values of n_a at 298°K and at the wavelengths 4880Å and 6328Å may be interpolated from the data given in Reference 22:

	KDP	KD*P	
n_a/n_c =	1.5155/1.4730	1.5114/1.4712	at 4880Å
	1.5075/1.4670	1.5041/1.4654	at 6328Å

In Table 1, however, only the following set of averaged values is used for all temperatures for which the temperature deviation in the range of our interest is estimated to be less than 0.4%:

KDP	KD*P	
n_a = 1.52	n_a = 1.51	at λ_o = 4880Å
n_a = 1.51	n_a = 1.50	at λ_o = 6328Å

After the above parameters are determined, V_π is easily obtained.

Table 1 clearly indicates the advantages of the transition temperature operation: both the half-wave voltage and the effective crystal thickness are greatly reduced with respect to their room temperature values, leading to much better resolution and a voltage range easier to work with. Since for KDP and KD*P the half-wave voltage and the effective crystal thickness are almost the same near their transition temperatures, KD*P is more favored because of its higher transition temperature.

4. THERMAL CONSIDERATIONS

KDP is a fairly soft material and, in the form of a thin platelet, is extremely fragile. This requires the crystal to be mounted on a substrate for support. The crystal assembly is as follows. One face of the crystal is coated with a cadmium oxide semitransparent, conducting layer (to act as a reference plane of potential) and is cemented by means of silicone cement to a calcium fluoride substrate. A multilayer dielectric coating is deposited on the opposite face, so that light incident from the substrate side is totally reflected, making two passes through the crystal. This type of operation, usually referred to as the reflex mode, will be discussed in Chapter 5.

When the crystal is cooled down to its transition temperature, thermal considerations such as thermal expansion, heat dissipation and thermal conduction are of paramount importance. The thermal expansion coefficients should be well matched; high thermal conductivities are needed to conduct away the heat dissipated in the crystal. These items are dealt with in the following sections.

4.1 Heat Generation

The heat power generated by stopping the incoming electron beam is roughly the product of the accelerating potential and the beam current. At room temperature this is about 0.3 watt, by comparison with which the radiation heat transfer is negligibly small.[3] However, if the crystal is to be maintained near its transition temperature, such as -55°C for KD*P, the thermal radiation effect is no longer negligible. On the contrary, the radiation heat input will become large and dominate, due to the larger

temperature difference between the crystal and its surroundings. A rough estimate can be made using the Stefan-Boltzmann law. The radiation heat input, P_r, is calculated from the following expression[23]:

$$P_r = e\sigma AF_{12}(T_2^4 - T_1^4) \qquad T_2 > T_1, \ T \text{ in } {}^\circ K \tag{16}$$

where $\sigma = 5.664 \times 10^{-12}$ watts/cm^2/$^\circ$K^4 is the Stefan-Boltzmann constant, A is the area of the crystal surface at temperature T_1, e is the emissivity ($1 \geq e > 0$), and F_{12} ($1 \geq F_{12} \geq 0$) is the so-called "view factor", which is 1 when the T_1 surface is convex and completely enclosed by the T_2 surface. Using

$$e = 1, \ F_{12} = 1, \ T_2 = 300^\circ K, \ A = 2\text{" square} = (5.08 \text{ cm})^2$$

the following results are computed:

T_1 ($^\circ$K)	P_r/AC (watts/cm^2)	$2P_r$ (watts)
200	.0368	1.90
208	.0353	1.82
213	.0342	1.77
218	.0331	1.71
223	.0319	1.65
228	.0307	1.59

Hence it is seen that the thermal radiation heat input over one side of the crystal substrate is approximately one watt, giving a total of two watts, which is much greater than the heat generated by electron beam bombardment alone.

4.2 Thermal Conductivities and Thermal Expansion Coefficients

Some data on the thermal conductivities and thermal expansion coefficients of elements of the crystal assembly are listed in Reference 3. However, they are room temperature values. For the crystal assembly to perform well when cooled down to the transition temperature, low temperature data are indispensable. These are given in the following figures.

a) Figure 7 gives the thermal expansion coefficient of CaF_2 as a function of temperature.[24]

b) Figure 8 gives the thermal conductivity of CaF_2 as a function of temperature.[25]

c) Figure 9 shows the temperature dependence of the lattice constants of KDP (and KD*P if the temperature axis is shifted) as a function of temperature. The crystal is unclamped. The curves show the change of the lattice constants, in units of 10^{-2} Å, with respect to the room temperature (293°K) values in various crystallographic directions.[26] Above the transition temperature the crystal has a tetragonal structure ($a_1 = a_2$), while below the transition temperature it becomes orthorhombic causing an elongation of a and a compression of b.[26] The linear thermal expansion coefficient can be obtained from the following:

$$\alpha = \frac{1}{(L_0 + \Delta L)} \frac{dL}{dT} \simeq \frac{1}{L_0} \frac{\Delta L}{\Delta T}$$

where L_0 is the room temperature reference value of the lattice constants, $\frac{\Delta L}{\Delta T}$ is the ratio of lattice deviation over the temperature difference between the temperature of interest and the room temperature. Using

$$a_1 = a_2 = a = 10.508\ \text{Å},\ c = 6.970\ \text{Å} \text{ at } 293^\circ\text{K for KDP}$$

the following average values are obtained[26]:

$$\frac{1}{a}\frac{da}{dT} = 2.0 \times 10^{-5}$$

$$\frac{1}{c}\frac{dc}{dT} = 4.2 \times 10^{-5}$$

where the former value is of our interest since the crystal is constrained in the ab-plane.

d) Figure 10 shows the thermal conductivities of KDP and KD*P as a function of temperature.[27]

It is seen that CaF_2, besides having good optical quality and high thermal conductivity, matches KD*P well near the transition temperature, as far as the thermal expansion is concerned. Also, the thermal conductivities of KDP and KD*P are almost constant near and above their respective transition temperatures.

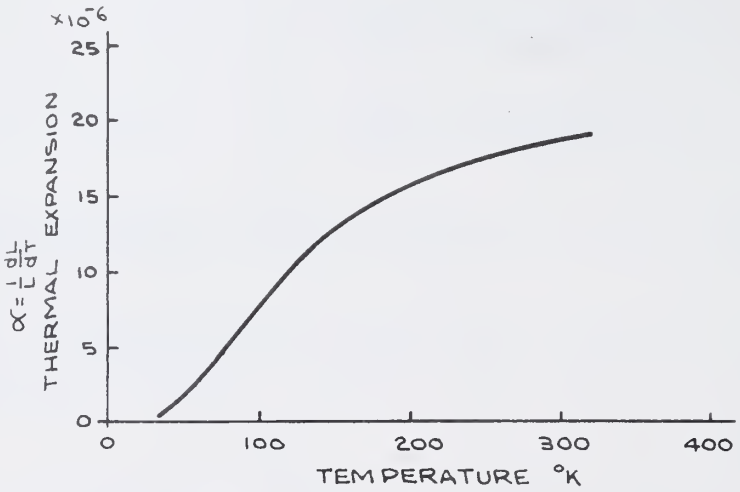

Figure 7. Thermal Expansion Coefficient of CaF_2 as a Function of Temperature

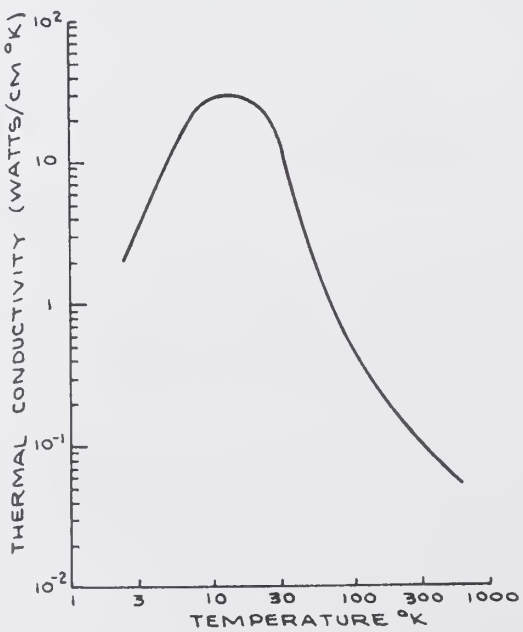

Figure 8. Thermal Conductivity of CaF_2 as a Function of Temperature

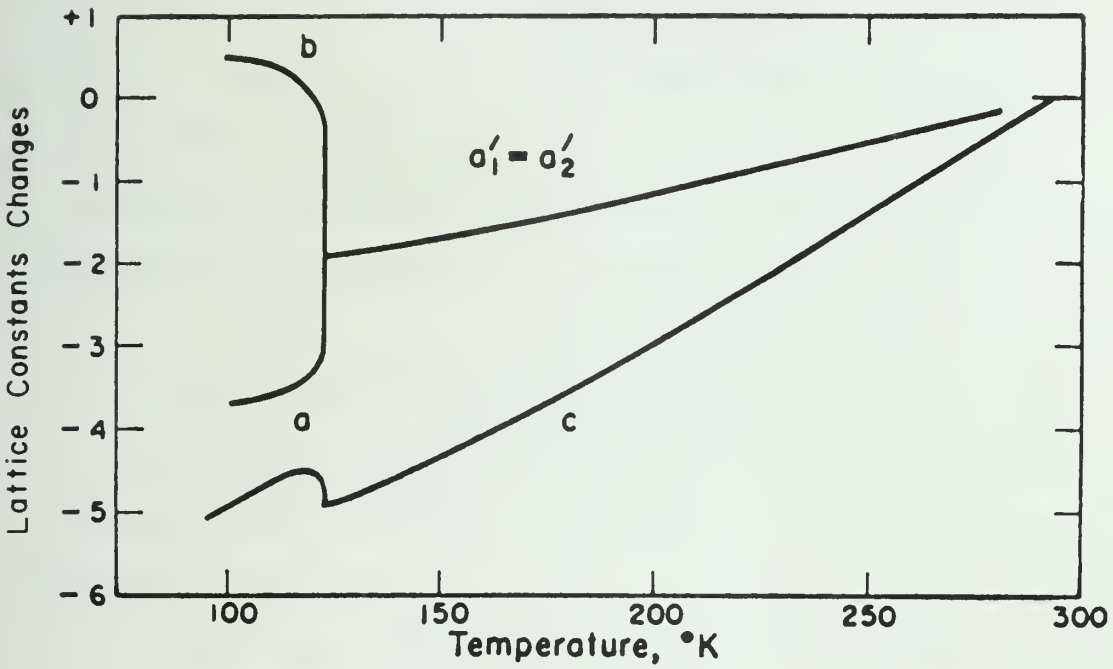

Figure 9. Change of Lattice Constants of KDP Versus Temperature

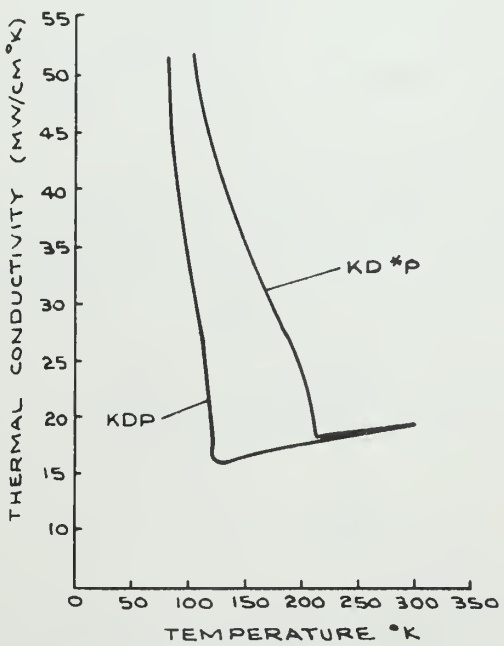

Figure 10. Thermal Conductivities of KDP and KD*P as a Function of Temperature

4.3 Temperature Variation over the Crystal Surface

The homogeneity of the electro-optic properties is affected by the temperature variation over the crystal surface since ϵ_c at points of different temperature may differ considerably. From Figure 6 it is seen that the uniformity of the electro-optic properties could be maintained near the transition temperature, if the temperature of the entire crystal surface is kept within an approximate range of $4^{\circ}C$.

The large amount of heat radiation absorbed by the crystal assembly, together with the heat generated by the electron beam on the crystal surface, can cause large temperature variations over the crystal surface. The temperature variations due to electron energy dissipation and due to thermal radiation are found separately and then added, using the superposition principle, to give the total temperature distribution.

To simplify the calculations a rectangular geometry is assumed, as shown in Figure 11. A, B and C are the dimensions of the substrate, whose thermal conductivity is denoted by h. The crystal has dimensions 2D x 2E, centered on one face of the substrate. Since the crystal thickness is very small compared with D and E, transverse heat flow in the crystal can be neglected and temperature differences calculated for the substrate surface will also apply to the crystal itself. The side faces of the substrate are assumed to be maintained by a cooling device at a constant (zero) temperature. Thus, the problem is to solve the Laplacian

$$\nabla^2 T = 0 \qquad (17)$$

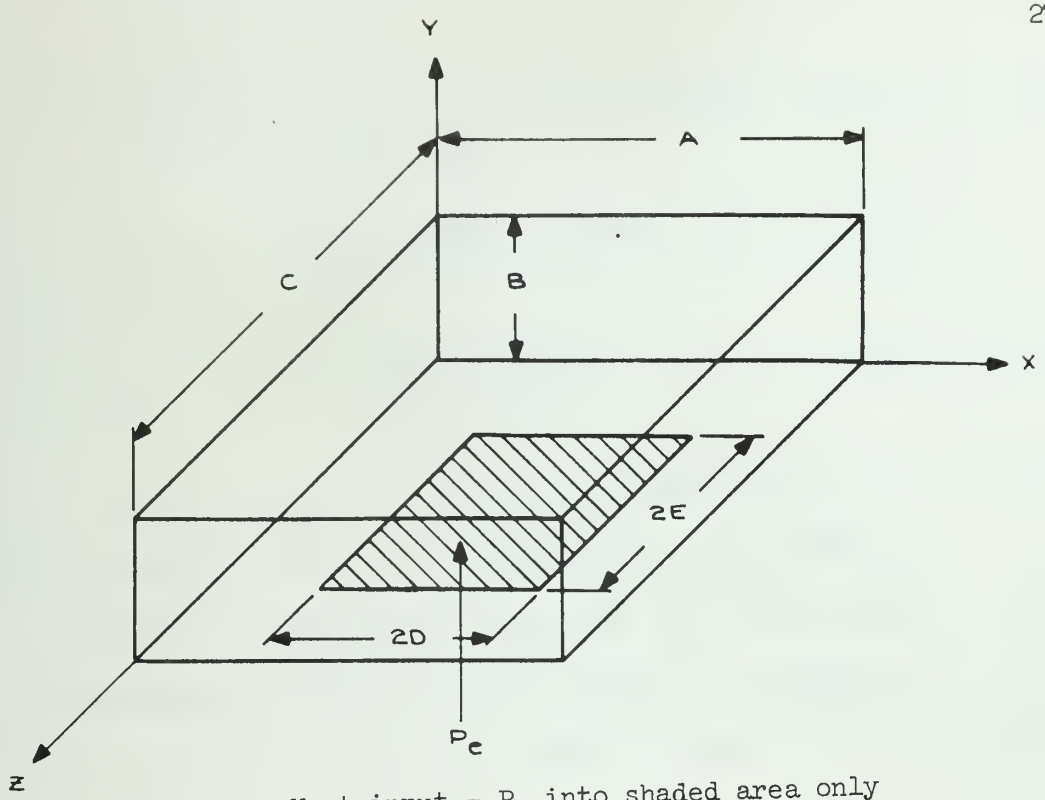

Problem 1: Heat input = P_e into shaded area only

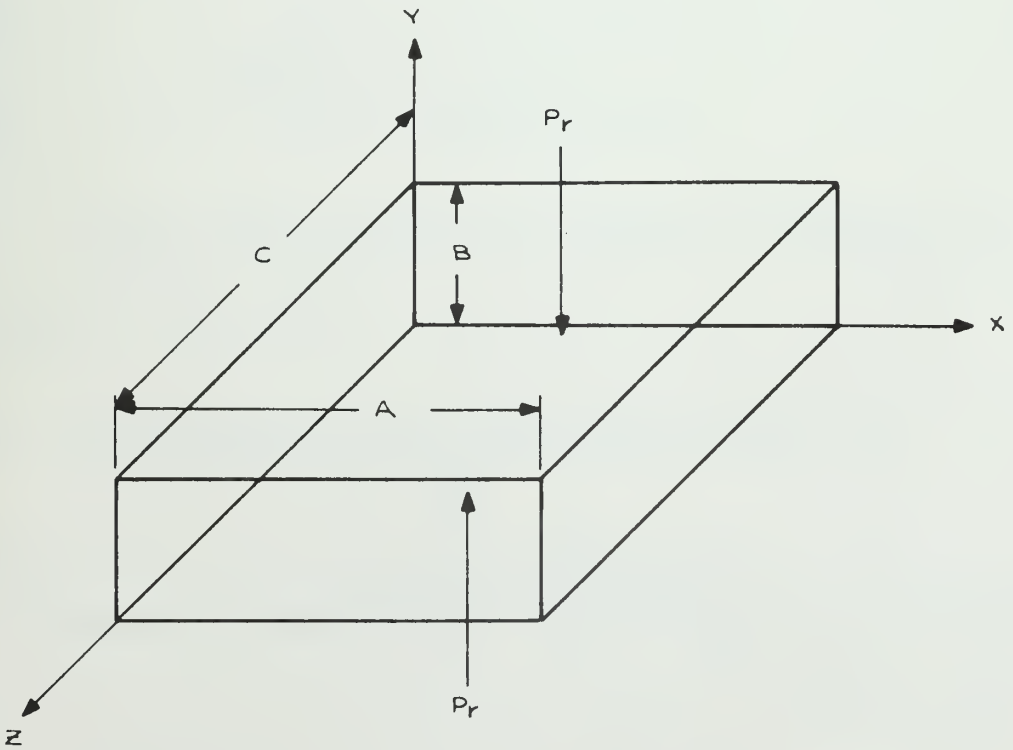

Problem 2: Heat input = P_r into top and bottom face

Figure 11. Temperature Variation Problem

within the substrate, subject to

$$T(x = \overset{0}{A}, y, z) = T(x, y, z = \overset{0}{C}) = 0 \tag{18}$$

and other boundary conditions, as given below.

Problem 1: Electron Bombardment at P_e watts.

In a hypothetical worst case no heat is lost from the substrate through the y = B face. Also, the power P_e absorbed due to electron bombardment is assumed to be spread uniformly over the crystal surface. Thus, the additional boundary conditions are

$$\frac{\partial}{\partial y} T(x, y = B, z) = 0 \tag{19}$$

$$\frac{\partial}{\partial y} T(x, y = 0, z) = \begin{cases} -P_e/4DEh \text{ on the crystal} \\ 0 \text{ elsewhere} \end{cases} \tag{20}$$

By separation of variables, the general solution of (17) satisfying (18) is

$$T_e(x,y,z) = \sum_{m,n=1}^{\infty} [A_{mn} \exp(\lambda_{mn} y) + B_{mn} \exp(-\lambda_{mn} y)] \sin(\frac{m\pi x}{A}) \sin(\frac{n\pi z}{C}) \tag{21}$$

where

$$\lambda_{mn} = \pi(\frac{m^2}{A^2} + \frac{n^2}{C^2})^{\frac{1}{2}} \tag{22}$$

The coefficients A_{mn} and B_{mn} are determined by applying (19) and (20) to (21). A few simple integrations[28] yield the result

$$T_e(x,y,z) = \frac{4P_e}{DEh\pi^2} \sum_{\substack{m,n \\ \text{odd}}} (-1)^{\frac{1}{2}(m+n-2)} \frac{1}{mn}$$

$$x \sin\left(\frac{m\pi D}{A}\right) \sin\left(\frac{m\pi x}{A}\right) \sin\left(\frac{n\pi E}{C}\right) \sin\left(\frac{n\pi z}{C}\right)$$

$$x \frac{\cosh[\lambda_{mn}(B-y)]}{\lambda_{mn}\sinh(\lambda_{mn}B)} \tag{23}$$

Problem 2: Thermal Radiation of P_r/AC watts/cm^2 Each Face.

In this case the power density is again assumed constant. This is justified if the temperature variation over the crystal surface is small compared with the mean temperature difference between substrate and surroundings. Boundary conditions (19) and (20) must now be replaced by

$$\frac{\partial}{\partial y} T(x,y = B,z) = P_r/ACh \tag{24}$$

$$\frac{\partial}{\partial y} T(x,y = 0,z) = -P_r/ACh \tag{25}$$

Obtaining the solution to (17) then follows the same lines as in Problem 1. The result is

$$T_r(x,y,z) = \frac{16P_r}{ACh\pi^2} \sum_{\substack{m,n \\ \text{odd}}} \frac{1}{mn} \sin\left(\frac{m\pi x}{A}\right) \sin\left(\frac{n\pi z}{C}\right)$$

$$x \frac{\exp(\lambda_{mn}y) + \exp[\lambda_{mn}(B-y)]}{\lambda_{mn}[\exp(\lambda_{mn}B) - 1]} \tag{26}$$

Note that T_e, given by (23), reduces to T_r, given by (26), as $P_e \rightarrow P_r$, $2D \rightarrow A$, $2E \rightarrow C$ and $B \rightarrow B/2$. This is to be expected (and is in fact a useful check), since these transformations make both boundary value

problems the same. Mathematically, therefore, Problem 2 can be regarded as a special case of Problem 1.

Using the expressions (23) and (26) and the symmetry of Figure 11, the maximum temperature variation over the crystal surface can be obtained by calculating the difference of the values of $T(x,0,z)$ at the corner and the center points of the crystal surface:

$$\begin{aligned} \Delta T_e &= T_e\left(\frac{A}{2},0,\frac{C}{2}\right) - T_e\left(\frac{A}{2}+D,0,\frac{C}{2}+E\right) \\ \Delta T_r &= T_r\left(\frac{A}{2},0,\frac{C}{2}\right) - T_r\left(\frac{A}{2}+D,0,\frac{C}{2}+E\right) \\ \Delta T_{total} &= \Delta T_e + \Delta T_r \end{aligned} \tag{27}$$

A program was written to compute the temperature differences (27) from the expressions (23) and (26) for various substrate dimensions. The following values were constant throughout the calculations:

$$\begin{aligned} D &= E = 0.5" \\ P_e &= 0.2 \text{ watt} \\ P_r/AC &= 0.0387 \text{ watts/cm}^2 \\ h &= 9.65 \text{ watts/m/}^\circ\text{C} \end{aligned}$$

The results are summarized in Table 2. As can be seen, they are well within the allowable 4°C range and should therefore prove acceptable.

DIMENSIONS	A = C = 1.5"	A = C = 2"	A = C = 3"
B = 3/8"	0.30 0.29 0.59	0.30 0.31 0.61	0.32 0.32 0.64
B = 1/2"	0.26 0.24 0.50	0.28 0.24 0.52	0.28 0.24 0.52
Total Power In (watts)	1.3	2.2	4.7

Table 2. Computed Maximum Crystal Surface Temperature Variation for Different Substrate Dimensions. (Three figure groups represent ΔT_e, ΔT_r and ΔT_{total} from top to bottom.)

4.4 Cooling Considerations

The most obvious way of cooling the crystal assembly would be to circulate a refrigerant around the substrate periphery. In this case a refrigeration unit with a mechanical pump is necessary. The transmission of mechanical vibration to the crystal assembly is unacceptable, however, since the Pockels tube is part of a video information processing system. Thermoelectric cooling, sometimes called solid state cooling, in which the refrigeration is accomplished by passing a dc current through the device without the use of a refrigerant and mechanically moving parts, is hence suggested. Thermoelectric cooling devices utilize the well known Peltier effect[29,30] which is a reversible phenomenon involving the interchange of heat and electrical energy. When a circuit composed of two dissimilar conductors carries an electric current, heat is absorbed at one junction and emitted at the other. Thus it is possible to construct a cooling device using the Peltier effect if proper materials are available and proper electrical and thermal connections are arranged.

A thermodynamic treatment of the theory of thermoelectric cooling shows[29] that the coefficient of performance and the maximum temperature drop attainable by thermoelectric cooling depend strongly on a parameter Z, called the figure of merit, given by[29]

$$Z = \frac{\alpha^2}{\rho K} \tag{28}$$

where α is the Seebeck coefficient, ρ is the electrical resistitivity and K is the thermal conductivity. Figure 12 shows that semiconductors have higher figures of merit than metals and insulators.[29] Bi_2Te_3 and its alloys have been found to exhibit the most desirable characteristics for operation near ambient temperatures.[30] A typical thermoelectric cooling module assembly is shown in Figure 13. The P-type and N-type materials used are typically Bi_2Te_3-Sb_2Te_3 and Bi_2Te_3-Sb_2Se_3.

Heat is absorbed at the cold junction and emitted at the hot junction at a rate proportional to the carrier current and the number of couples in the module. To pump more heat many couples are usually connected electrically in series and thermally in parallel such as shown in Figure 13, which represents a single stage. Such stages can be further connected in series thermally to increase the temperature difference between the hot side and the cold side. However, as the number of stages increases, the physical size of the module becomes impractically large and heat extraction capacity becomes smaller though the temperature difference is increased.[30]

The Pockels tube dimensions are likely to limit the usable cooling modules to two stage devices. Calculations[31] show that a small device should be able to extract about 0.2 watt with cold/hot temperatures of approximately

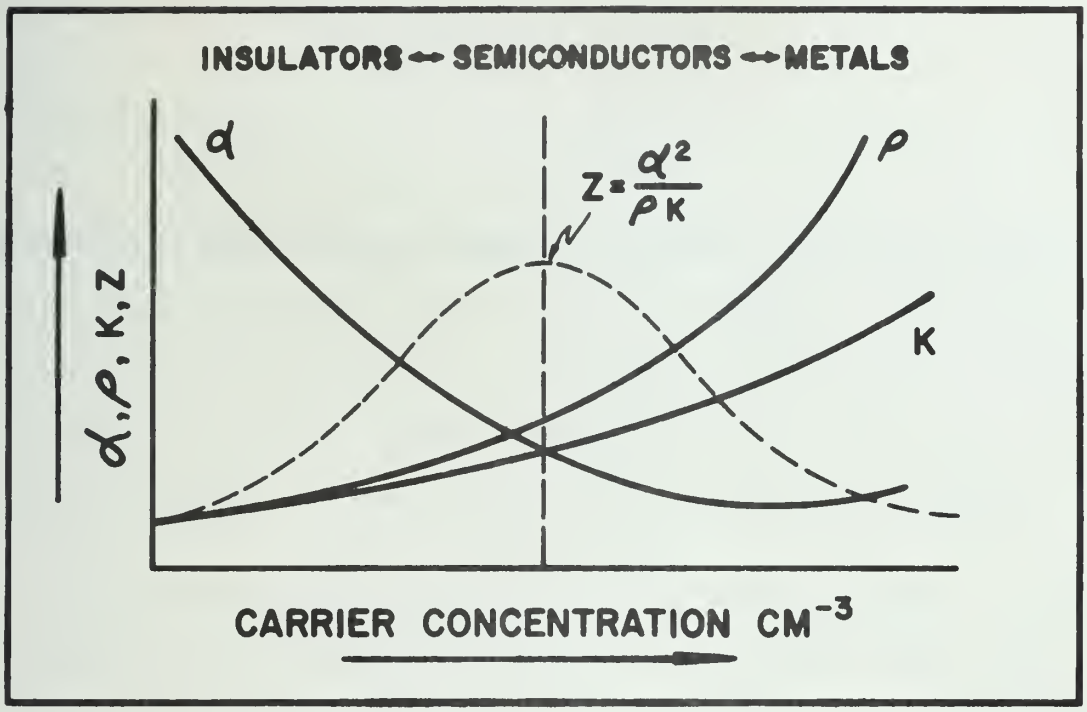

Figure 12. Figure of Merit of Thermoelectric Elements as a Function of Carrier Concentration

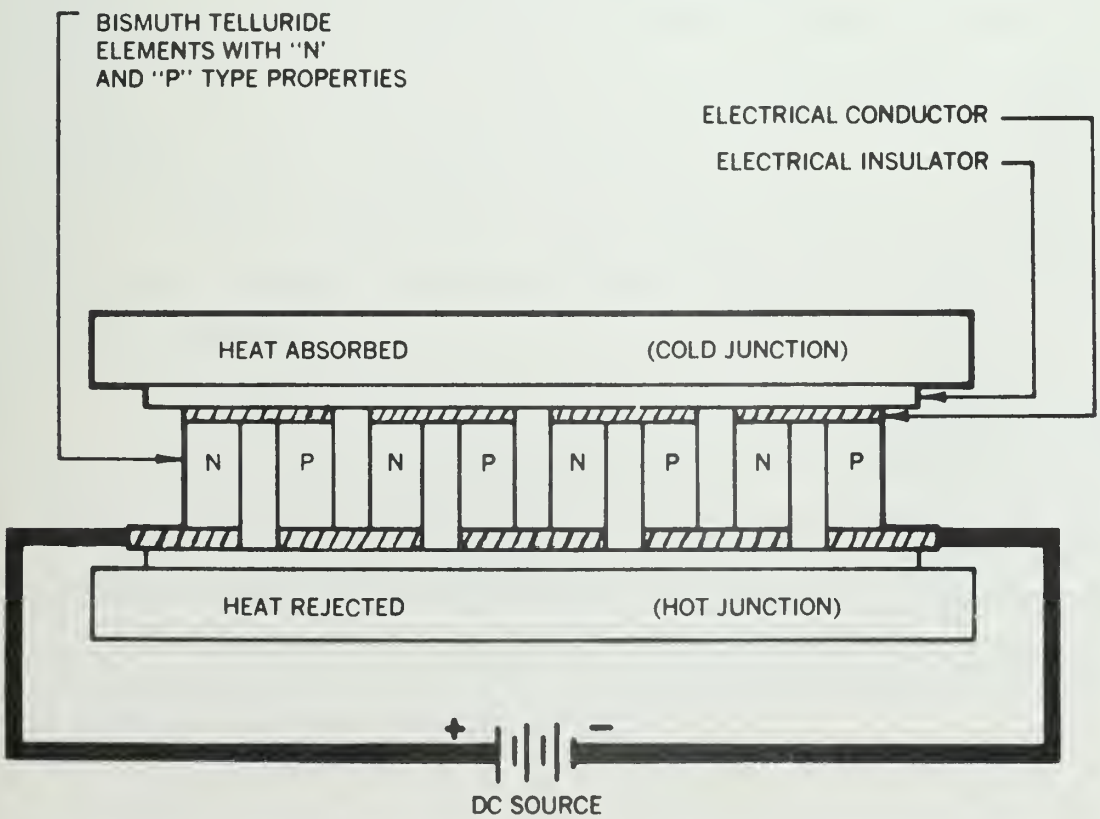

Figure 13. Typical Thermoelectric Cooling Module Assembly

-70/0°C

-60/15°C

-55/27°C

It seems just possible that an array of somewhat larger devices (~ 6 x 0.4 watts) can be designed into the system.

5. REFLEX MODE OPERATION

5.1 Pros and Cons

There are two basic ways of designing a Pockels tube. In the transmission mode, shown in Figure 14, both the light and the electron beam are incident on the same side of the crystal assembly. The other scheme is referred to as the reflex mode, Figure 15, in which the light and the electron beam are incident from opposite directions. Both configurations display certain advantages and disadvantages, which will now be discussed.

a) The transmission mode allows the simpler crystal assembly. No dielectric reflection (mirror) coating is required on the exposed crystal face. Such a coating has the electrical effect of introducing a series capacitance in the target circuit, which necessitates an increase in the electron accelerating potential over what is otherwise required to produce half-wave voltage across the crystal. This is a series disadvantage at ambient temperatures where the half-wave voltage is of the order of kilovolts. But near the transition temperature the half-wave voltage has fallen to about 200 volts, so that an additional voltage drop across the mirror capacitance is quite tolerable.

b) In the reflex mode the light makes a double pass through the crystal and therefore experiences twice the phase change, for a given applied voltage, over that obtainable in the transmission mode. The half-wave voltage is equivalently lower in the reflex mode by a factor of 2. However, the mechanical tolerances on flatness and parallelism of crystal and substrate surfaces are tighter by the same factor.

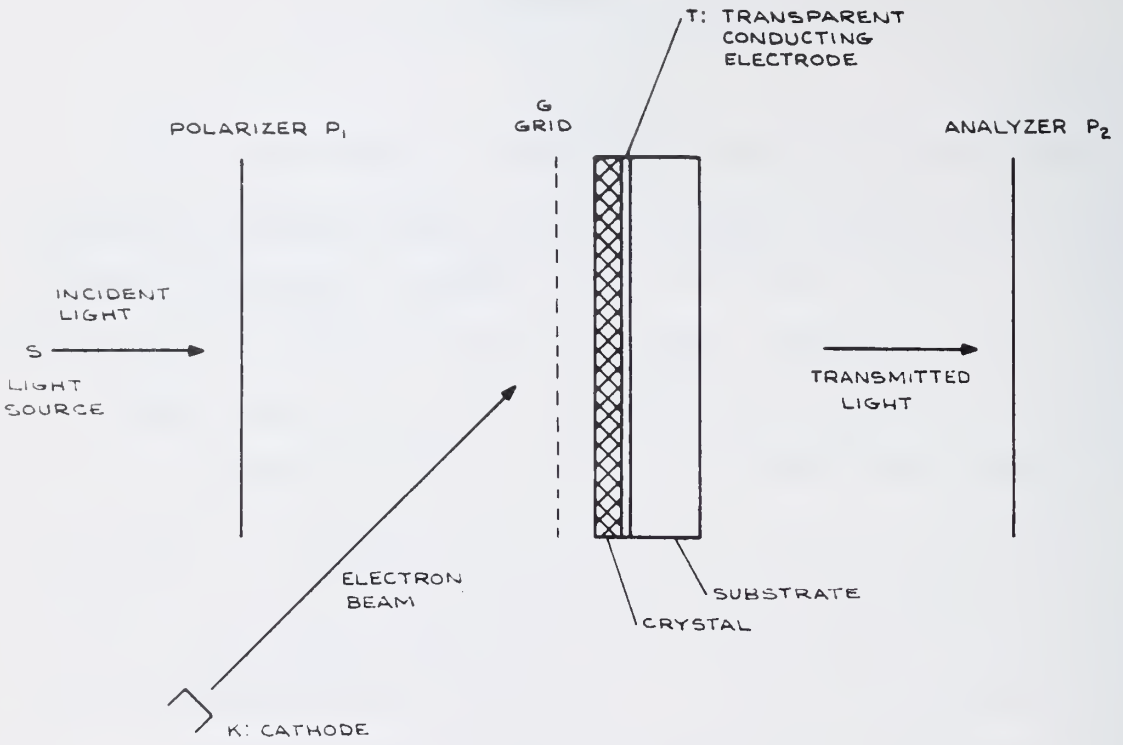

Figure 14. Transmission Mode Configuration of Pockels Tube

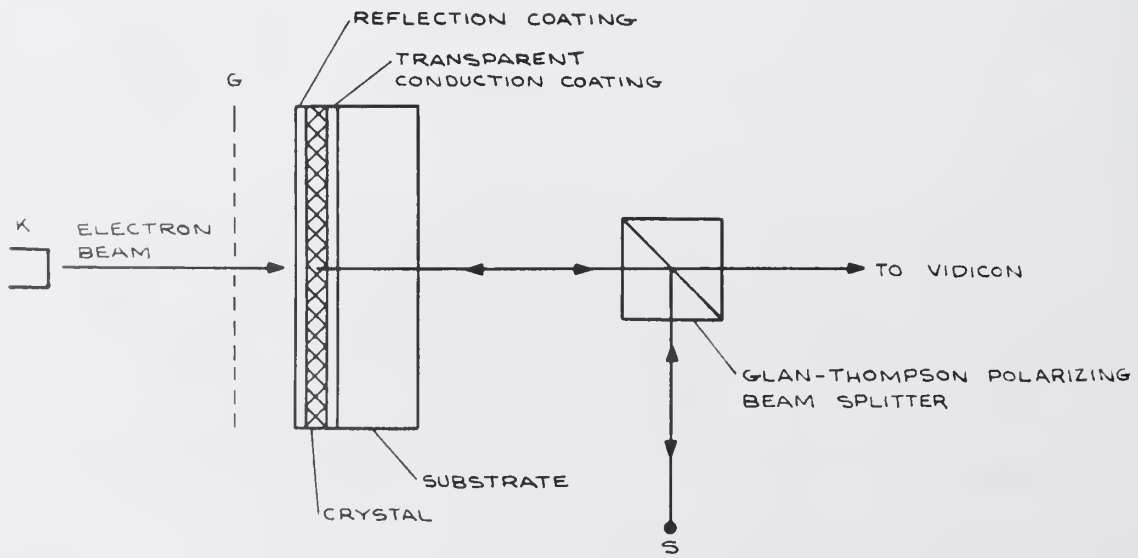

Figure 15. Reflex Mode Configuration of Pockels Tube

c) In the transmission mode the electron gun must usually be offset from the optical axis so as not to interfere with the light path. This leads to a "keystoned" and imperfectly focused image. Correcting these effects requires extensive modification of the sweep and focus circuitry. In the reflex mode these problems are avoided because both light and electron beam can impinge on the crystal at normal incidence.

d) At ambient temperatures the charge decay time constant of the crystal is commensurate with video frame rates, so that it is not absolutely necessary to provide means for charge erasure between successive frames. But the time constant is so long near the transition temperature as to necessitate erasure by controlled secondary emission. A secondary emission mesh grid placed close to the crystal surface introduces severe diffraction effects in the transmission mode, but has obviously no optical effect in the reflex mode where it is out of the light path.

Thus, it is seen that the reflex mode is more suitable for a transition temperature system.

5.2 Crystal Coating

5.2.1 Optical Considerations

For high optical efficiency in the reflex mode two features are important: a dielectric reflection coating[32,33,34] must be deposited on the crystal surface, and the incident light should be introduced via a good quality polarizing (e.g. Glan-Thompson) prism, which also receives the reflected light and separates out the desired polarization component.

The reflectance of a surface may be considerably enhanced by the deposition of a single film of high refractive index material having an optical thickness of $\frac{\lambda_0}{4}$ at the wavelength at which the high reflectance is desired. The refractive index of the film should exceed that of the substrate.[34] The reflectance of a surface of refractive index n_2 covered by a $\frac{\lambda_0}{4}$ film of index n_1 is[32]

$$R = \left(\frac{n_0 n_2 - n_1^2}{n_0 n_2 + n_1^2}\right)^2 \qquad (29)$$

For an antireflection coating, $n_1 = (n_0 n_2)^{\frac{1}{2}}$ is used. Conversely, to have high reflection n_1 needs to be high. Table 3 gives the reflectance of a surface of index 1.5 (glass) when covered by a single $\frac{\lambda_0}{4}$ film of commonly used high refractive index materials. If the substrate is KD*P, $n_2 = 1.5$ at $\lambda_0 = 4880$ Å. Then using $n_1 = 2.6(TiO_2)$, for example, R is calculated to be 0.4.

Much higher reflection can be achieved by using a "quarter-wave stack"[33]. It consists of a series of thin films of alternating high and low refractive index, each being a quarter-wave optical length thick. The usual arrangement is as shown in Figure 16. High refractive index layers are next to the substrate and at the air interface. Some common high and low refractive index materials are listed in Tables 3 and 4. The indices vary with deposition conditions; hence values in Tables 3 and 4 are only representative.

Material	n	λ Å	R
Uncoated Glass	1.5	5461	0.04
ZnS	2.3	5461	0.31
TiO_2	2.6	5461	0.40
Sb_2S_3	2.7	10000	0.43
Ge	4.0	20000	0.69
Te	5.0	40000	0.79

Table 3. Reflectance (R) of Glass with Various Quarter-Wave Coatings

Material	n
Na_3AlF_6 (cryolite)	1.35
CaF_2	1.28
MgF_2	1.38
$ThOF_2$	1.52
CeF	1.63

Table 4. Refractive Index of Various Low Index Materials at 6000°A

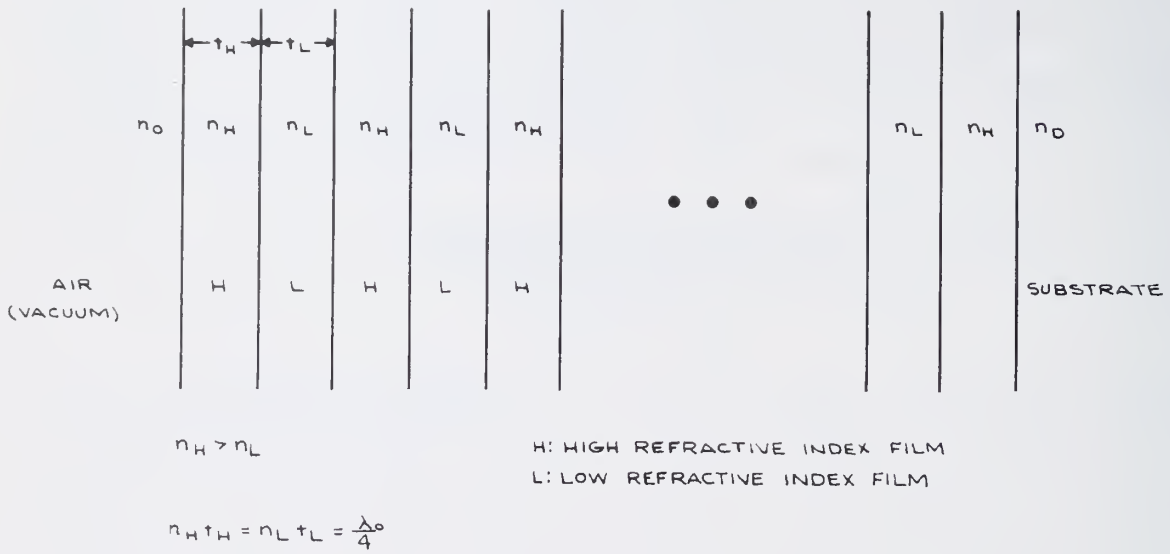

Figure 16. Quarter-Wave Stack Reflection Coating

The reflectance at a given wavelength can be computed from either the expressions in Reference 32 or the hyperbolic tangent expression in Reference 34. Computed results of reflectance of quarter-wave stacks listed in Table 5[36] show how multilayer coatings increase the maximum reflectance.

It is seen that in the visible region, the zinc sulphide and cryolite combination is the most effective. In fact, this combination has been widely used for many years. But, cryolite is sometimes rejected because it is mechanically weak and water-soluble. Instead, magnesium fluoride evaporated in high vacuum is the material mostly used nowadays, because mechanically robust and chemically stable films can be made from it.[34,35]

System	No. of layers	CeO_2 + cryolite, $\lambda = 0.55\mu$	Sb_2S_3 + CaF_2, $\lambda = 1\mu$	Ge + cryolite, $\lambda = 2\mu$	ZnS + cryolite, $\lambda = 0.589\mu$
DH	1	0.35	0.447	0.69	
DHLH	3	0.73	0.835	0.96	0.695
DHLHLH	5	0.91	0.900	0.99	0.891
DHLH	7	0.97	0.977		0.964
DHLH	9		0.995		0.988
DHLH	11		0.999		0.998
		$n_D = 1.52$	$n_D = 1.45$	$n_D = 1.45$	$n_D = 1.50$

Table 5. Reflectance of Quarter-Wave Stacks

No information about the spectral characteristics is given in Table 5. However, Figure 17 shows some representative curves for stacks of (ZnS, MgF_2).[33]

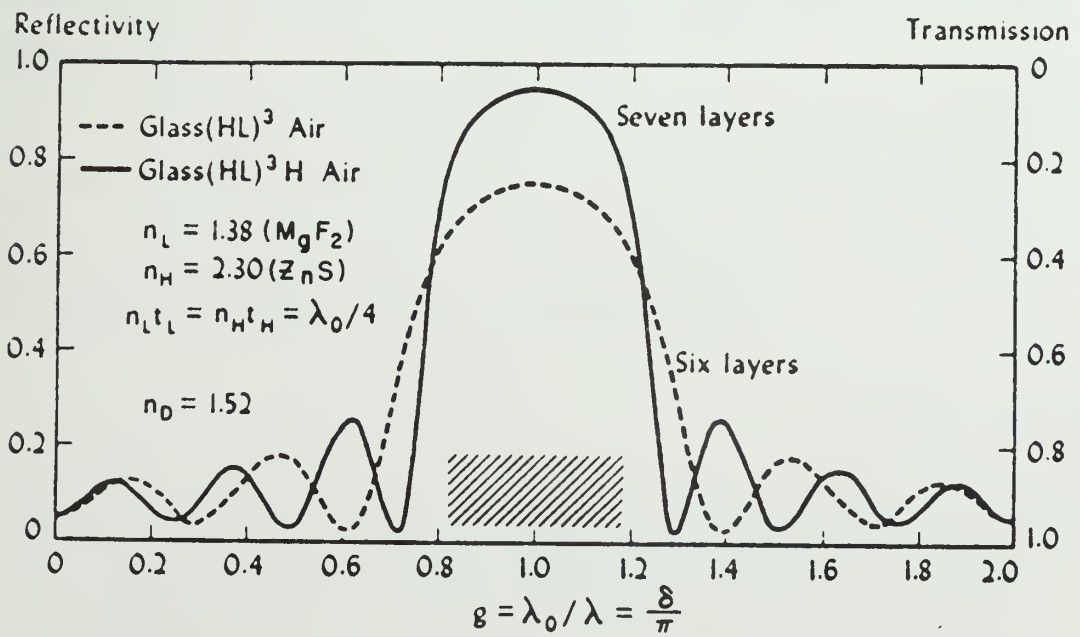

Figure 17. Reflectance of ZnS + MgF_2 Quarter-Wave Stacks

5.2.2 Electrical Considerations

The multilayer thin films in the quarter-wave stack act as a series of capacitors in series with the crystal capacitor, as can be seen from Figure 16 where the substrate in our case is the KD*P crystal. The voltage dividing effect is, assuming ideal capacitors, expressed in the following simple derivations.

For convenience let us assume there are m layers of thin films where m is taken to be an even number. The total capacitance of the thin films is C_F expressed by

$$\frac{1}{C_F} = \frac{m}{2}\left(\frac{1}{C_H} + \frac{1}{C_L}\right) = \frac{m}{2\epsilon_0 A}\left(\frac{t_H}{\epsilon_H} + \frac{t_L}{\epsilon_L}\right) \tag{30}$$

The capacitance of the crystal is $C_X = \epsilon_0 \epsilon_x \frac{A}{t_x}$. Hence, the voltage across the crystal V_X is related to the voltage across the reflection films V_F by

$$\frac{V_X}{V_F} = \frac{C_F}{C_X} = \frac{2t_x}{m\epsilon_x\left(\frac{t_H}{\epsilon_H} + \frac{t_L}{\epsilon_L}\right)} \tag{31}$$

Since for the quarter-wave stack

$$n_H t_H = n_L t_L = \frac{\lambda_0}{4} \tag{32}$$

equation (31) becomes

$$\frac{V_X}{V_F} = \frac{C_F}{C_X} = \frac{8t_x}{m\epsilon_x\lambda_0\left(\frac{1}{\epsilon_H n_H} + \frac{1}{\epsilon_L n_L}\right)} \tag{33}$$

Using the following data[36] in (33):

$$m = 8, \quad \lambda_0 = 0.6328\mu$$
$$n_H = 2.3, \quad \epsilon_H = 8.5 \qquad (ZnS)$$
$$n_L = 1.38, \quad \epsilon_L = 4.9 \qquad (MgF_2)$$
$$t_x = 5 \text{ mil} = 127\mu, \quad \epsilon_x = 650 \qquad (KD*P)$$

we obtain

$$\frac{V_X}{V_F} = 1.55 \tag{34}$$

For maximum modulation, $V_X = V_\pi/2 \simeq 132$ volts near the transition temperature of KD*P. Then (34) yields

$$V_F = 85 \text{ volts} \tag{35}$$

corresponding to a total voltage across the crystal-coating assembly of about 217 volts.

The foregoing results can also be used to calculate the maximum voltage across individual film layers. This is about 5 and 16 volts for zinc sulphide and magnesium fluoride, respectively, which are probably below the breakdown voltages for these materials.[36]

6. SUMMARY

The present work has been the investigation of the principal factors involved in the design of a transition temperature Pockels tube. The general features of the transition temperature operation of an electro-optic light valve have been discussed in Chapter 2 and further analyzed in more detail in Chapter 3, where typical numerical values have been obtained and comparisons made. The necessity of a uniform electro-optical response of the crystals has led in turn to the requirement of maintaining a near uniform temperature over the crystal surface. Consequently in Chapter 4 the thermal problems have been considered, which include the discussion of heat generation, thermal expansion match, temperature distribution and variation, and a possible cooling device. Finally, since the reflex mode operation of light offers significant advantages over the transmission mode, the properties of the reflection coating have been discussed in Chapter 5. All those subjects define the major design factors for a transition temperature Pockels tube to be developed in the Department of Computer Science at the University of Illinois, under the supervision of Professor W. J. Poppelbaum and Professor M. Faiman.

LIST OF REFERENCES

1. A. Yariv, "Quantum Electronics", John Wiley and Sons, New York, 1967.

2. E. J. Calucci, "Solid State Light Valve Study," 5th National Symposium, Society for Information Display, February, 1965.

3. W. J. Poppelbaum, M. Faiman, D. Casasent, and D. Sand, IEEE Proceedings, 56, 744, 1968. For more detail, see: D. P. Casasent, "An On-Line Electro-Optical Video Processing System," (Ph.D. Thesis) Report No. 331, Department of Computer Science, University of Illinois, Urbana, Illinois, May, 1969.

4. E. Lindberg, et al., "Solid State Beam Controlled Light Modulator," AD413403, Motorola, Chicago, 1963. Rome Air Development Center Contract No. AF 30(602)-2645.

5. R. S. Stites, et al., "Electro-Optic Projection Study," AD617087, Autonetics, Anaheim, California, 1965. Rome Air Development Center Technical Report No. RADC-TR-65-25.

6. W. E. Stoney, "Electro-Optic Projector Study," C6-1256/34, Autonetics, Anaheim, California, 1966. Final Report on Rome Air Development Center Contract No. AF30(602)-3720.

7. R. Peterson, "Development of a Light Valve Cathode Ray Tube," AD149001, Wiley Electronics, Phoenix, Arizona, 1957. Final Report on Signal Corps Contract No. DA 36-039 SC-72399.

8. F. Jona and G. Shirane, "Ferroelectric Crystals," Pergamon Press, New York, 1962.

9. W. Kanzig, "Ferroelectrics and Antiferroelectrics," in Solid State Physics, Vol. 4, ed. by F. Seitz and D. Turnbull, Academic Press, New York, 1957.

10. C. Kittel, "Introduction to Solid State Physics," John Wiley, New York, Third Edition, 1966.

11. S. Wang, "Solid State Electronics," McGraw-Hill, New York, 1966.

12. I. P. Kaminow, Physical Review, 138, A1539, 1965.

13. B. Zwicker and P. Scherrer, Helvetica Physica Acta, 17, 346, 1944.

14. D. Sand, "A Theoretical Analysis of the Modulation Characteristics of an Electro-Optic Light Valve," (MS Thesis) Report No. 303, Department of Computer Science, University of Illinois, Urbana, Illinois, January, 1969.

15. W. P. Mason, "Piezoelectric Crystals and Their Applications in Ultrasonics," Van Nostrand, New York, 1950.

16. G. Busch, Helvetica Physica Acta, 11, 269, 1938.

17. T. R. Sliker and S. R. Burlage, Journal of Applied Physics, 34, 1837, 1963.

18. H. Baumgartner, Helvetica Physica Acta, 24, 326, 1951.

19. R. M. Hill and S. K. Ichiki, Physical Review, 130, 150, 1963.

20. G. Marie, Philips Research Reports, 22, 110, 1967.

21. I. P. Kaminow and E. H. Turner, Applied Optics, 5, 1612, 1966.

22. R. A. Phillips, Journal of the Optical Society of America, 56, 629, 1966.

23. R. B. Bird, et al., "Transport Phenomena," John Wiley and Sons, New York, 1960.

24. A. C. Baily and B. Yates, Proceeding of Physical Society (London), 91, 390, 1967.

25. G. A. Slack, Physical Review, 122, 1451, 1961.

26. M. de Quervain, Helvetica Physica Acta, 17, 509, 1944.

27. Y. Suemune, Journal of the Physical Society of Japan, 22, 735, 1967.

28. H. S. Carslaw and J. C. Jaeger, "Conduction of Heat in Solids," Oxford University Press, Oxford, 1959.

29. A. F. Ioffe, "Semiconductor Thermoelements and Thermoelectric Cooling," translated by Infosearch Ltd., London, 1957.

30. R. K. Heikes and R. W. Ure, Jr., "Thermoelectricity: Science and Engineering," Interscience, New York, 1961.

31. Data on thermoelectric cooling modules from Cambridge Thermionic Corp., Nuclear System, Inc., Borg-Warner Corp., and Material Electronic Products Co.

32. O. S. Heavens, "Optical Properties of Thin Solid Films," Dover Publications, New York, 1965.

33. R. Kingslake, ed., "Applied Optics and Optical Engineering, Volume I: Light, Its Generation and Modification," Academic Press, New York, 1965.

34. H. Anders, "Thin Films in Optics," translated by J. N. Davidson, the Focal Press, London, 1967.

35. L. Holland, "Vacuum Deposition of Thin Films," Chapman and Hall Ltd., London, 1963.

36. K. L. Chopra, "Thin Film Phenomena," McGraw-Hill, New York, 1969.